PCCP

Symmetry and ^{1}H NMR chemical shifts of short hydrogen bonds: Impact of electronic and nuclear quantum effects

Journal:	*Physical Chemistry Chemical Physics*
Manuscript ID	CP-ART-12-2019-006840
Article Type:	Paper
Date Submitted by the Author:	19-Dec-2019
Complete List of Authors:	Zhou, Shengmin; Rutgers The State University of New Jersey, Chemistry and Chemical Biology Wang, Lu; Rutgers The State University of New Jersey, Department of Chemistry and Chemical Biology

PCCP

ARTICLE TYPE

Cite this: DOI: 00.0000/xxxxxxxxxx

Symmetry and ^{1}H NMR chemical shifts of short hydrogen bonds: Impact of electronic and nuclear quantum effects†

Shengmin Zhou[a] and Lu Wang*[a]

Received Date
Accepted Date

DOI: 00.0000/xxxxxxxxxx

Short hydrogen bonds (SHBs), which have the donor and acceptor separations below 2.7 Å, occur extensively in small molecules and proteins. Due to their compact structures, SHBs exhibit prominent covalent characters with elongated Donor–H bonds and highly downfield ($>$ 14 ppm) ^{1}H NMR chemical shifts. In this work, we carry out first principles simulations on a set of model molecules to assess how quantum effects determine the symmetry and chemical shift of their SHBs. From simulations that incorporate the quantum mechanical nature of both the electrons and nuclei, we reveal a universal relation between the chemical shift and the position of the proton in a SHB, and unravel the origin of the observed downfield spectral signatures. We further develop a metric that allows one to accurately and efficiently determine the proton position directly from its ^{1}H chemical shift, which will facilitate the experimental examination of SHBs in both small molecules and biological macromolecules.

1 Introduction

The three-dimensional architecture of proteins often creates specialized structural elements, notably hydrogen bonds that are much shorter than those typically observed in the condensed phases.[1–6] These short hydrogen bonds (SHBs) have the donor-acceptor heavy atom distances, R, below 2.7 Å and are associated with a wide variety of biological processes, ranging from enzyme catalysis to cellular signal transduction.[7–14] For example, X-ray and neutron diffraction experiments have revealed that in the presence of the an antibiotic ligand, a SHB forms between two catalytic residues in the enzyme aminoglycoside N3-acetyltransferase-VIa.[12] This SHB, which has R of 2.57 Å and the proton almost equally shared between the donor and acceptor atoms, is proposed to facilitate the enzymatic acetyl transfer reactions and mediate the bacterial antibiotic resistance.[12] From a statistical analysis of the top 1% highest-quality structures in the Protein Data Bank (PDB),[15,16] we have recently shown that SHBs are prevalent in biological macromolecules and many of them exist in the active site of proteins, indicating their functional importance.[6]

In a SHB A–H$\cdots$B, the donor and acceptor atoms reside much closer than the sum of their van der Waals radii. As such, SHBs exhibit prominent covalent characters, in stark contrast to the standard description of hydrogen bonds as classical dipole-dipole interactions. For example, electronic quantum effects such as exchange repulsion, induction and dispersion play major roles in determining their interaction energies.[5,17,18] By examining 3665 SHBs that form from amino acid side chains, we find that the barrier for proton transfer decreases with R and hence nuclear quantum effect, such as zero-point energy and tunneling, can significantly alter their properties.[6] In particular, when R is between 2.4 and 2.6 Å, one enters the low-barrier hydrogen bond regime where the zero-point energy of an O–H or N–H bond becomes comparable to the potential energy barrier and allows the proton to be delocalized in the hydrogen bond.[7,8,19] The quantum nature of the SHBs manifest as distinct geometric and spectroscopic properties. For example, it is well known that the A–H covalent bond is significantly elongated when R decreases.[20,21] From neutron diffraction of small molecule crystals, researchers have observed symmetric O–H$\cdots$O hydrogen bonds that has the proton centered between the O atoms when R is below 2.45 Å.[20–25] Accordingly, the stretching frequency of an A–H bond shifts from its regular value of about 3500 cm^{-1} to below 800 cm^{-1} when R reduces from 2.8 to 2.4 Å.[26–30]

One of the most distinctive features of SHBs is their far downfield ^{1}H chemical shifts, δ_H, in the nuclear magnetic resonance (NMR) spectra. While hydrogen atoms in typical functional

[a] Department of Chemistry and Chemical Biology, Institute for Quantitative Biomedicine, Rutgers University, Piscataway, NJ 08854, USA.

† Electronic Supplementary Information (ESI) available: Computational determination of the ^{1}H NMR chemical shifts and supplementary figures. See DOI: 10.1039/b000000x/

‡ E-mail: lwang@chem.rutgers.edu

groups have δ_H below 10 parts per million (ppm), lengthening of the A–H bonds in SHBs deshields the protons and shifts their δ_H values to more than 14 ppm.[7,8,14,31–36] For example, serine proteases utilize a highly conserved Asp–His–Ser triad in the active site to catalyze the hydrolysis of peptide bonds[37] and the length of the Asp–His hydrogen bond is often below 2.7 Å.[6] The δ_H values of this SHB vary from 18.6 to 19.0 ppm in chymotrypsin, a classic serine protease, depending on the structure of the inhibitor in the active site.[38] Similarly, the Asp–His SHB exhibits a chemical shift of 17.4 ppm in subtilisin E and 19.9 ppm in a serine protease from the Dengue type II virus.[13,39] Accompanying the downfield δ_H, one often observes small deuterium (D) fractionation factors from the NMR experiments of SHB-containing proteins. As the fractionation factor is the equilibrium constant for the H/D isotope exchange between protein and water, a value lower than 1 suggests that the lighter isotope H is enriched in the biological SHB while the heavier D is more likely to exist in the solvent molecules. Note that the fractionation factor would be 1 if the nuclei were classical particles, and hence it directly uncovers the impact of nuclear quantum effects on the structures and properties of biological SHBs.[8,31,32,38,39]

Despite the importance of SHBs in proteins, dissecting their symmetry and ^{1}H chemical shifts is highly challenging due to the experimental difficulty to probe specific protons in a large biomolecule. To tackle this problem, researchers have examined a series of organic and inorganic small molecules that contain a single SHB to unravel the common properties of these compact structures. A famous example is the compound 1,8-bis(dimethylamino)naphthalene (DMAN), also known by its trade name Proton Sponge.[40,41]. DMAN is an exceptionally strong base with $pK_a = 12.3$ and has a weak nucleophilic character due to its highly strained structure.[40,41] Protonation releases this steric strain and the resulting cation, DMANH, contains a stable intramolecular N–H$\cdots$N hydrogen bond with R of 2.55–2.63 Å and $\delta_H > 17$ ppm.[42,43] Other examples include the salts of hydrogen maleate (HM)[7,38,44] and 4,5-dihydroxynaphthalene-2,7-disulfonate (DHND),[45,46] which serve as model systems for the O–H$\cdots$O type SHBs, and *cis*-urocanic acid (CUA), which has been designed to mimic the Asp–His SHB in serine proteases.[7] The chemical structures of the 4 model molecules are depicted in Fig. 1. By measuring the X-ray diffraction patterns and NMR spectra of these small molecules, researchers have identified a strong correlation between δ_H and R and utilized this relation to obtain the hydrogen bond lengths in proteins.[32,46–50] However, as the lengths of the O–H or N–H bonds are only available for a few systems, how δ_H depends on the proton positions in the SHBs has not been established. While electronic structure calculations have provided crucial insights into this problem,[51–53] they are carried out on the optimized configurations of the small molecules or proteins and hence neglecting the critical influences from structural fluctuations and nuclear quantum effects.

In this work, we consider DMANH, HM, DHND and CUA in organic solvents and aqueous solutions and utilize *ab initio* molecular dynamics (AIMD) and *ab initio* path integral molecular dynamics (AI-PIMD) simulations to investigate how quantum effects determine the symmetry and chemical shifts of their SHBs. As shown in Fig. 1, these molecules form stable intramolecular hydrogen bonds with R $<$ 2.6 Å and exhibit large downfield ^{1}H chemical shifts, providing excellent models for N–H$\cdots$N, O–H$\cdots$O and O–H$\cdots$N SHBs in proteins.[7,43–45,54–57] The first principles simulations evolve the nuclear motion from on-the-fly electronic structure calculations and allow the chemical bonds to dynamically form and break as the conformations of the compounds fluctuate. In addition, AI-PIMD simulations effectively incorporate the quantum nature of the nuclei using the path integral formalism of quantum mechanics, which exploits the isomorphism between the partition function of a quantum mechanical system and a classical system of ring polymers.[58–60] Hence a direct comparison between the AIMD and AI-PIMD trajectories unravels how the interplay of electronic and nuclear quantum effects impacts the structure, proton sharing conditions and ^{1}H chemical shifts of the SHBs. By extracting representative configurations from the simulations, we further establish a relation between δ_H and the position of the proton and elucidate the origin of the highly downfield chemical shifts for the SHBs.

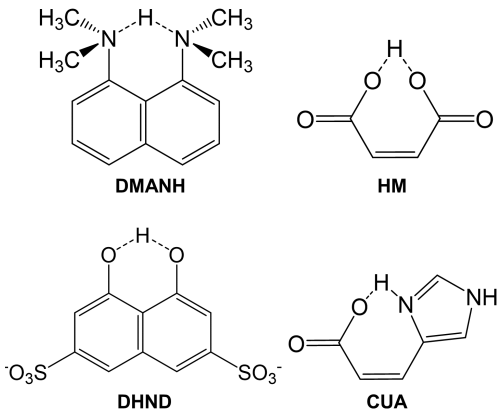

Fig. 1 Chemical structures of the model molecules that contain intramolecular SHBs.

2 Computational Methods

We obtained the structures of the 4 model molecules from the Cambridge Structural Database[61] and solvated them using the Amber 2016 software package[62] to form the following systems: DMANH in acetonitrile and in water, HM in acetone and in water, DHND in water and CUA in dimethyl sulfoxide (DMSO). The solvation was carried out by placing 1 DMANH, HM and CUA in 86 acetonitrile, 62 acetone and 66 DMSO molecules, respectively. The aqueous solutions of DMANH, HM and DHND contained 1 solute molecule in 151, 185 and 160 waters, respectively. As DMANH, HM and DHND possessed net charges, sodium or chloride ions were added to neutralize the system. For each solvated structure, the simulations were performed in a cubic box with periodic boundary conditions, and the box length varied between 17 and 25 Å to ensure that the system had the correct solvent density at the temperature of the corresponding experimental NMR measurements. The simulation temperatures were 300 K for DMANH in acetonitrile and CUA in DMSO, 298 K for DMANH in water, 268 K for DHND in water, and 308 K for HM in acetone and wa-

ter.[7,44,45,54–57]

As a first step, we equilibrated the systems with classical molecular dynamics (MD) simulations using the Amber 2016 package.[62] The potential energies of the solute and organic solvent were modeled using the general AMBER force field[63] and the water molecules were described with the TIP3P model.[64] The SHAKE algorithm was used to constrain all the bonds that involved hydrogen atoms,[65] and the particle-mesh Ewald method was implemented to treat long-range electrostatic interactions.[66] After energy minimization, each system was equilibrated with a constant pressure at 1 bar and a constant temperature using the Langevin thermostat[67] and Berendsen barostat.[68] The equilibration was carried out for 4 ns with a time step of 2 fs. We took the final configuration of each system from the MD simulations and used them for the first principles simulations.

AIMD and AI-PIMD simulations were performed using the Quickstep module in the CP2K package[69] for the on-the-fly evaluations of the electronic structures and the i-PI software[70] for the propagation of the nuclear motion. For each system, the electronic structures were described using the BLYP density functional[71,72] with the D3 dispersion correction.[73] The Goedecker-Teter-Hutter pseudopotentials[74] were chosen to describe the core electrons and the DZVP-GTH plane-wave basis set with a cutoff of 300 Ry was used for the valence charge density. The simulations were performed in the canonical ensemble at a time step of 0.5 fs. In AIMD simulations, the stochastic velocity rescaling method[75] was applied to keep the temperature at the desired values. In AI-PIMD simulations, each atom was represented by 6 ring polymer beads using the path integral generalized Langevin equation method.[76] Each system was equilibrated for 10 ps, followed by AIMD simulations for 50 ps or AI-PIMD simulations for 25 ps.

From the AIMD and AI-PIMD simulations of DMANH, HM and DHND in aqueous solutions, we analyzed the hydrogen bonds between the solute molecules and water. We considered a pair of A–H$\cdots$B to be hydrogen bonded if its R $<$ 3.5 Å and the A–H–B angle $\theta_{AHB} > 135^{\circ}$. For all systems, we also calculated the average residence time of a proton in a SHB. Here we defined the residence time as the duration that the proton was closer to the donor or acceptor side before hopping happened, and the reported values were averaged over the donor and acceptor atoms and over the simulation trajectories.

To compute the ^{1}H NMR chemical shifts of the model molecules, we extracted configurations of the solute-solvent clusters every 100 fs from the AIMD simulations, and every 50 fs from the AI-PIMD simulations by randomly selecting one ring polymer bead. We included all solvent molecules that were within 5.5 Å of any atom of the solute and the resulting clusters contained 143–330 atoms. We then computed the ^{1}H NMR chemical shift of the solute-solvent clusters using the Gauge-Independent Atomic Orbital (GIAO) method,[77–79] as implemented in the Gaussian 16 software package.[80] The calculations were carried out using the B3LYP density functional,[81] the D3 dispersion correction[73] and the 6-31+G(d,p) basis set. The δ_H value of tetramethylsilane (TMS) at the same level of theory is 31.6 ppm and is subtracted from the values of the molecules to produce the chemical shifts. To elucidate the electronic quantum effects in the SHBs and how they lead to the downfield chemical shifts, we carried out the Natural Bond Orbital (NBO) analysis of DMANH with the NBO 6.0 software.[82] Here we used the optimized structures of DMANH and scanned the lengths of the A–H or B–H bonds in the gas phase. For each scanned configuration, we optimized the position of all the H atoms while maintaining the positions of the heavy atoms, and then conducted NMR and NBO calculations. To decompose the total chemical shift into contributions from covalent bonds and hydrogen bonds, we repeated the NMR calculations on the compound N,N-dimethylaniline, which was chosen to model the donor and acceptor groups in DMANH. For this purpose, we removed the atoms from the other half of the DMANH molecules and added two H atoms to saturate the bonds of the C atoms in N,N-dimethylaniline. The coordinates of these H atoms were optimized while the positions of all the other atoms were fixed. We then took the same proton positions in the hydrogen bond of DMANH in the scan process and carried out NMR calculations. The overall shielding constant from covalent bonding was computed as the sum of the chemical shifts from the donor and acceptor groups. The shielding constant of hydrogen bonding was calculated as the difference between the total shielding and that from covalent bonding.

3 Results and Discussion

3.1 Geometry and symmetry of the intramolecular SHBs

In a symmetric hydrogen bond, the proton is centered between the donor and acceptor groups. It has been proposed that the formation of a symmetric hydrogen bond requires 1) a short distance between the hydrogen bond partners (R $\leq$ 2.5 Å), 2) a matched proton affinity of the donor and acceptor atoms, and 3) a non-aqueous environment.[83,84] By examining the 4 model molecules, we will elucidate how these criteria arise from the quantum nature of the hydrogen bonds.

As a first step, we evaluate the impact of R on the geometry and symmetry of the SHBs and use a coordinate ν to characterize the proton positions in these compounds. For DMANH, HM and DHND, we define $\nu = d_{X_1H} - d_{X_2H}$, where X is N or O and d_{X_1H} and d_{X_2H} are the distances from the hydrogen atom to the two equivalent heavy atoms in the SHBs. For CUA, we take this coordinate as $\nu = d_{OH} - d_{NH}$. From its definition, $\nu = 0$ means that the proton equally bridges the donor and acceptor groups, leading to a symmetric hydrogen bond, whereas a negative or positive ν shows that the proton is closer to the donor or acceptor groups, respectively. From the AIMD and AI-PIMD simulations, we compute the joint probability for finding the hydrogen bond at length R and the proton at position ν, $P(R,\nu)$. At a given temperature T, the free energies are calculated as

$$F = -k_B T \ln \frac{P(R,\nu)}{P_{max}}, \quad (1)$$

where k_B is the Boltzmann constant. P_{max} is the probability of the corresponding system at the most likely R and ν, and is included to ensure that the minimal free energy is 0. At thermal equilibrium, the molecules dynamically switch between different conformations and form an ensemble of hydrogen bonding geometries.

When these interconversions happen faster than the time scale of the NMR measurements, one would observe a symmetric hydrogen bond if the free energy surface is symmetric and the average ν is 0.

As Fig. 2a demonstrates, DMANH forms a relatively symmetric N_1–H$\cdots$$N_2$ hydrogen bond in acentonitrile from AIMD simulations. R of the hydrogen bond fluctuates between 2.4 and 2.9 Å and the energetically most favorable configuration has R = 2.7 Å and ν = -0.5 Å. A second minimum occurs symmetrically at R = 2.7 Å and ν = +0.5 Å, which is only 0.2 kcal/mol higher in energy compared to the most stable hydrogen bonding conformation. In the AIMD simulations, we observe frequent hopping of the proton in the SHB, consistent with the observations in previous Car-Parinello molecular dynamics simulations of DMANH in other environment.[85,86] However, there is a barrier of 2.4 kcal/mol connecting the 2 proton transferred configurations and hence the proton spends more time around the N_1 or N_2 atoms, rather than the middle of the SHB. From Fig. 2a, the absolute values of ν decrease almost linearly when R shortens from 2.9 Å to 2.4 Å, regardless of whether the proton is closer to N_1 ($\nu \leq 0$) or N_2 ($\nu > 0$). In other words, the hydrogen bond becomes more symmetric as the separation between N_1 and N_2 decreases. We have recently shown that electronic quantum effects give rise to this pronounced proton sharing in the SHBs, and calculations based on a classical force field can only provide a qualitative trend in lengthening the Donor–H bond.[6]

From Fig. 2b, inclusion of nuclear quantum effects significantly increases the region that the proton can move and washes out the double-well feature of the free energy profile. From AI-PIMD simulations, the most stable configuration of the SHB in DMANH has R of 2.6 Å and ν of 0.1 Å, where the proton resides nearly in the middle of the SHB. While shortening R again facilitates proton sharing in Fig. 2b, nuclear quantum effects allow the proton to be delocalized between the N_1 and N_2 atoms as it takes less than 0.7 kcal/mol to move the proton between ν of -0.5 and +0.5 Å. In the mean time, nuclear quantum effects also make the N_1–H–N_2 angle vary over a wide range of 114–180° in AI-PIMD simulations, as compared to 131–176° in AIMD simulations. This demonstrates the well-known competition of nuclear quantum effects in facilitating the N–H stretch motion, which strengthens the hydrogen bond, and enhancing the bending and rotational of the bonds, which weaken the hydrogen bonds.[87–91] For DMANH, the strengthening effect dominates as the average residence time of the proton on the two N atoms decreases from 0.15 ps in AIMD simulations to 0.04 ps in AI-PIMD simulations. The average residence time is inversely related to the proton exchange rate in the SHB, and the values from both simulations are much shorter than the millisecond time scale in a typical NMR experiment. Considering that the free energy surfaces in Figs. 2a and b have symmetric features and that the average ν is -0.05 and 0.01 Å when the nuclei are treated classically and quantum mechanically, respectively, both simulations predict that the SHB in DMANH is considerably symmetric in acetonitrile.

The chemical structure of DMANH has reflection symmetry about a plane that bisects the naphthalene ring (Fig. 1). Therefore, it is not surprising that in the organic solvent acetonitrile, the donor and acceptor atoms of the N–H$\cdots$N hydrogen bond have identical proton affinities and hence their pK_a mismatch, ΔpK_a, is 0. One can possibly perturb this pK_a matching condition by putting DMANH in aqueous solution. As shown in Figs. 2c and d, water molecules induce slight asymmetry in the distributions of the proton position. Comparing DMANH in acetonitrile and water, the solvent molecules do not form direct interactions with the N_1 and N_2 atoms due to the steric hindrance of the bulky methyl groups and the Cl^- counterions are 6–8 Å away from the N atoms, leading to minor influence on the proton positions. However, unlike acetonitrile, water forms slightly different solvation shells around the methyl groups of DMANH. From both the AIMD and AI-PIMD simulations, we find that the first solvation shells occur at a distance of 4.9 Å between the C atom in the methyl group and the O atom in water, and there are on average 15 and 16 water molecules in the first shells of the methyl groups surrounding the N_1 and N_2 atoms, respectively, leading to the slight asymmetry in the free energy surfaces.

Similar to DMANH, HM possesses reflection symmetry in its structure (Fig. 1) and its O_1–H$\cdots$$O_2$ hydrogen bond is highly symmetric in the organic solvent acetone. As shown in Fig. 2e, accompanying the structural fluctuations in the AIMD simulations, electronic quantum effects makes the proton more shared in the SHB when R decreases from 2.8 to 2.2 Å. The free energy surface exhibits two minima at R = 2.5 Å and $\nu = \pm 0.2$ Å. As the average R in HM is shorter than that in DMANH, the proton transfer barrier is only 0.4 kcal/mol, and as such, the zero-point energy associated with the O–H vibrations facilitates the quantum delocalization of the proton in the hydrogen bond. This is reflected in the free energy profiles in Fig. 2f, which has a single minimum with an average ν of 0.

In contrast, we observe prominent transient asymmetry in the SHB of HM in water, as demonstrated in Figs. 2g and h. From AIMD simulations of 50 ps, the most favorable hydrogen bonding conformation has R = 2.5 Å and ν = 0.4 Å and the average residence time of the proton on O_1 or O_2 is 0.09 ps. In the 25-ps AI-PIMD simulations, the interplay of nuclear and electronic quantum effects moves the minimum to ν = 0.2 Å and reduces the average residence time by 56%. In both cases, the most likely position of the proton is around the O_2 atom, rather than at the center of the hydrogen bond. Comparing HM in acetone and water (Figs. 2f and h), we expect the changes in the proton sharing conditions to arise from the distinct solute-solvent interactions. After examining the minimal-energy configuration of HM in aqueous solutions, we find that the O_1 and O_2 atoms have different solvation environment and form an average of 1.1 and 0.7 hydrogen bonds with the surrounding water molecules, respectively. 26% of these conformers accept 2 hydrogen bonds from water, 1 for each O atom, with a representative snapshot shown in Fig. 3a. 20% of them form only 1 hydrogen bond between O_1 and the solvent, as depicted in Fig. 3b. Apart from these commonly observed conformations, the SHB in HM can also take other solvation structures with the O_1 and O_2 atoms forming up to 3 hydrogen bonds with the water molecules. Therefore, although the ΔpK_a in the SHB of HM is 0 in a nonpolar environment, the heterogeneous hydrogen bonding patterns disturb its pK_a matching

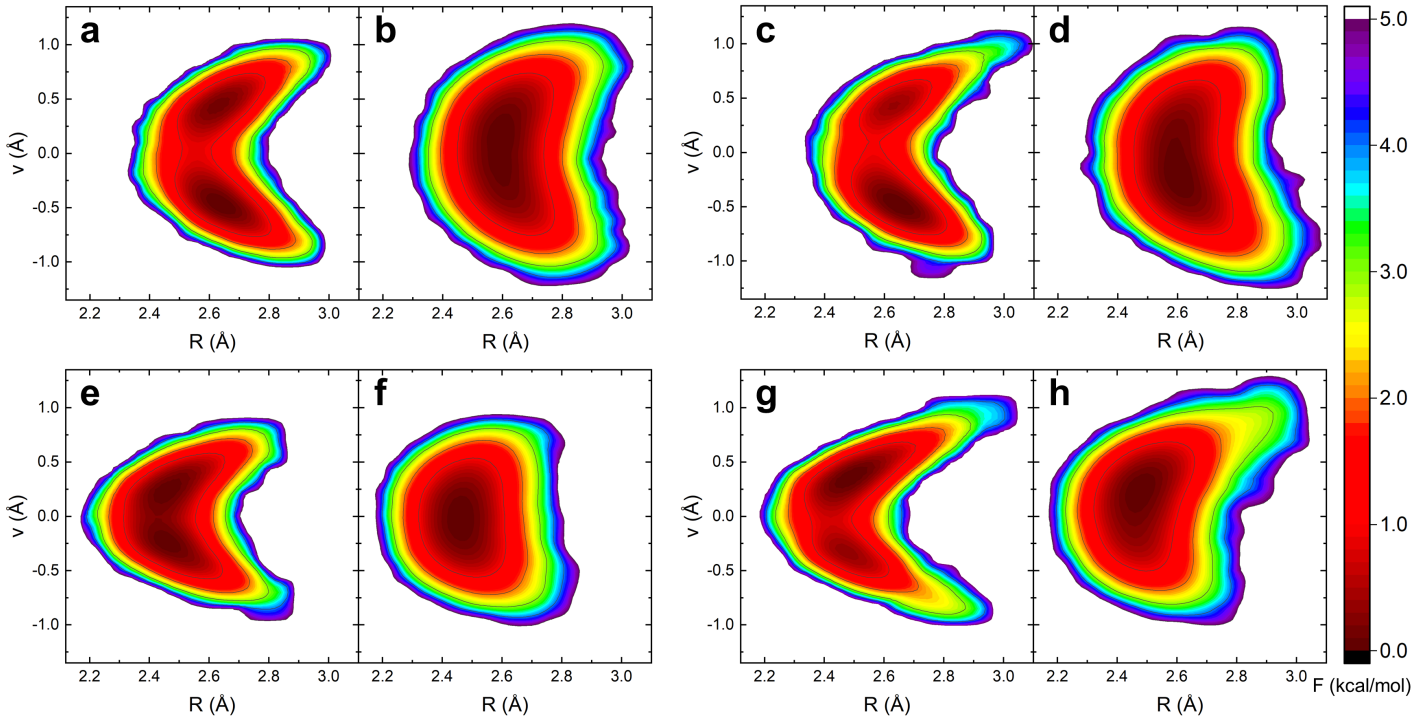

Fig. 2 Free energy profiles for DMANH and HM in organic solvents and aqueous solutions. In the top panels, the free energy surfaces are calculated from (a) AIMD and (b) AI-PIMD simulations of DMANH in acetonitrile, and from (c) AIMD and (d) AI-PIMD simulations of DMANH in water. In the bottom panels, the curves are calculated from (e) AIMD and (f) AI-PIMD simulations of HM in acetone, and from (g) AIMD and (h) AI-PIMD simulations of HM in water.

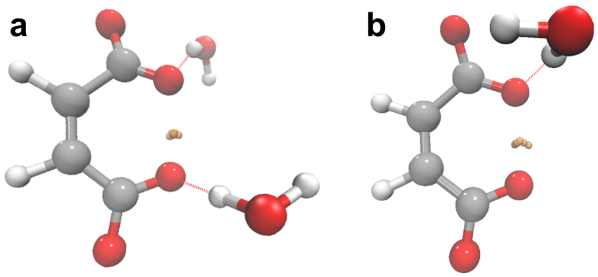

Fig. 3 Representative configurations of HM with the hydrogen bonded water molecules. The conformations have R of 2.5 Å and v of 0.2 Å. Silver, red and white represent C, O and H, respectively. The orange spheres are the ring polymer beads of the hydrogen bonded proton in HM.

condition and introduce asymmetry in its free energy surface. In particular, hydrogen bonding with water effectively reduces the proton affinity of the O atom, as our results and previous simulations both show that the proton is more likely to stay closer to the O that is less solvated.[92] It is important to note that the asymmetry in Figs. 2g and h is transient in nature as it reflects the instantaneous solvation environment around the O_1 and O_2 atoms. Although our simulations are not sufficiently long to fully sample the rearrangements of the water molecules, we expect the free energy surfaces to become symmetric in the time scale of the NMR measurements.

Similar to HM, the O_1–H$\cdots$$O_2$ hydrogen bond of DHND exhibit instantaneous asymmetry in water. From AIMD simulations, the O_1 and O_2 atoms form an average of 2.0 and 1.6 hydrogen bonds with the solvent molecules, respectively, which effectively introduces a nonzero ΔpK_a in its SHB. This is reflected in its free energy surface in Fig. 4a, which has a global minimum at R = 2.5 Å and v = 0.5 Å with the proton closer to the O_2 atom. A second minimum that is 0.4 kcal/mol higher in energy occurs at v of -0.5 Å. Although the average R of the intramolecular hydrogen bond is only 2.5 Å, DHND has a large barrier of 3.7 kcal/mol between the two minima and the average residence time of the proton is 0.56 ps. As shown in Fig. 4b, nuclear quantum effects enhance the transient asymmetry of the free energy surface. From AI-PIMD simulations, the ratio of solute-solvent hydrogen bonds for the O_1 and O_2 atom become 2:1 and accordingly, the proton spends 82% of the time closer to the less solvated O_2 atom ($v \geq 0$). In the mean time, nuclear quantum effects also promote proton sharing in the SHB as it takes only 1.2 kcal/mol to move the proton between -0.5 and +0.5 Å and the average residence time of the proton decreases to 0.11 ps.

To further evaluate how pK_a mismatch influences the properties of a SHB, we consider CUA, which possesses an intrinsic ΔpK_a of 3.7 between the imidazole and carboxylic groups,[56,93] and find that it has an asymmetric hydrogen bond. From AIMD simulations, its minimal-energy configuration occurs at R = 2.6 Å and v = -0.6 Å and electronic quantum effects give rise to a strong inverse correlation between v and R, as demonstrated in Fig. 4c. The proton is almost entirely attached to the O atom ($v < 0$) in the simulations, resulting in a long residence time of 1.16 ps. As shown in Fig. 4d, the proton can sample a much broader region in the hydrogen bond and the free energy minimum shifts to v =

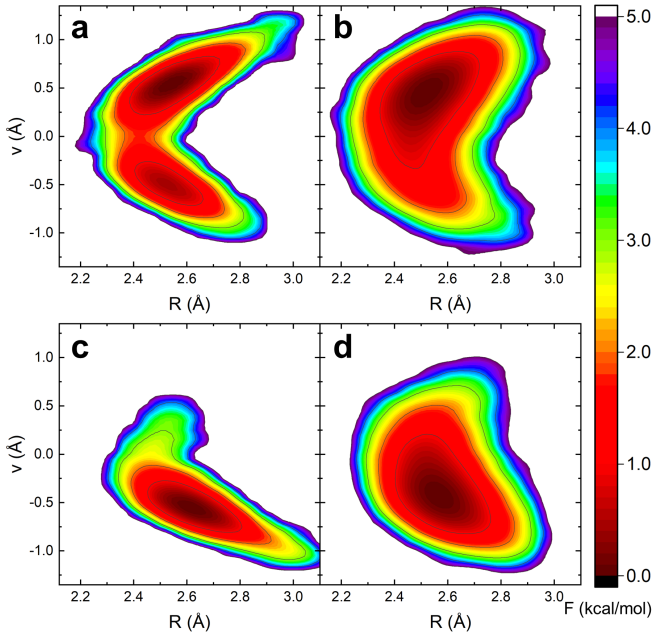

Fig. 4 Free energy profiles for DHND in water from (a) AIMD and (b) AI-PIMD simulations, and for CUA in DMSO from (c) AIMD and (d) AI-PIMD simulations.

-0.5 Å in AI-PIMD simulations. Upon addition of nuclear quantum effects, the proton becomes more shared in the SHB with a 13% probability of being transferred to the acceptor N atom ($\nu \geq 0$) and the average residence time is reduced to 0.09 ps, an order of magnitude shorter than that from the AIMD simulations.

From the first principles simulations, we now assess the proposed criteria for the formation of symmetric SHBs. First, electronic quantum effects facilitate proton sharing in a hydrogen bond when the distance between the donor and acceptor atoms decreases, as demonstrated by the free energy surfaces from the AIMD simulations. In the model molecules, the SHBs have R $\leq$ 2.7 Å and hence there are considerable probability of finding the proton around $\nu = 0$. Due to the short R, we observe that the protons frequently hop between the donor and acceptor groups and their average residence time is less than 1 ps, much shorter than the typical NMR time scale. As a result, what is measured from the NMR experiments is the ensemble average of the proton positions. Second, the pK_a matched condition, which depends on the intrinsic proton affinity of the donor and acceptor groups and the instantaneous solvation environment, is required for a symmetric hydrogen bond. For example, as DMANH, HM and DHND have reflection symmetry in their chemical structures, their ΔpK_a in the SHBs are 0 with no external perturbations. When these molecules are placed in aqueous solutions, the solute-solvent hydrogen bonds significantly modulate the ΔpK_a value of the SHBs and the protons are preferentially attached to the atom that is less solvated instantly, leading to transient asymmetry in their proton distributions.[83–86,92,94] In comparison, the SHB in CUA has an intrinsic ΔpK_a of 3.7 and a prominently asymmetric SHB, in which the proton spends 87% of the time around the donor O atom. Finally, AI-PIMD simulations closely mimic the experimental conditions as they include both electronic and nuclear quantum effects, and the interplay of these quantum effects plays a fundamental role in determining the symmetry of a SHB. From Figs. 2 and 4, nuclear quantum effects significantly enhance the region that the protons can move and shorten their average residence time on the N or O atoms by 60–92%. Notably, the influences of nuclear quantum effects are comparable to, if not greater than, those from R and ΔpK_a on the free energy surfaces and the proton behavior. Instead of experiencing electrostatic attraction by the donor and acceptor groups, the protons are quantum mechanically delocalized in the SHBs and the symmetry of the hydrogen bonds are enhanced.

3.2 ^{1}H NMR chemical shifts of the SHBs

From the AIMD and AI-PIMD simulations, we extract 6012 solute-solvent clusters of the model molecules and calculate their δ_H values using the B3LYP density functional,[81] the D3 dispersion correction[73] and the 6-31+G(d,p) basis set. As shown in Table 1, the average chemical shifts, $\langle\delta_H\rangle$, from the simulations are in good agreement with the experimental measurements. Considering that AI-PIMD simulations closely resemble the experimental conditions, the excellent comparison between their predicted chemical shifts and the experimental values validates our approach of combining these simulations and DFT calculations to obtain δ_H. From Table 1, we find that the chemical shifts from our calculations and experiments are all highly downfield ($>$ 16 ppm). In addition, the $\langle\delta_H\rangle$ values from the AI-PIMD simulations are systematically larger than those from the AIMD simulations by 0.3–2.1 ppm.

Pioneering first principles simulations have shown that one can use ν to effectively represent the electronic state of a hydrogen bond and link its structure to the chemical shielding on the protons.[95,96]. To uncover the molecular origin of the observed trends in Table 1, we use ν as a collective coordinate and decompose $\langle\delta_H\rangle$ into two components,

$$\langle\delta_H\rangle = \int_{-\infty}^{\infty} \delta_H(\nu)P(\nu)d\nu. \quad (2)$$

For a model molecule, $\delta_H(\nu)$ describes how its chemical shift changes with the proton position ν as its structure fluctuates, and $P(\nu)$ represents the probability distribution of ν in the SHBs. In the following, we will examine the two properties individually.

3.2.1 Universal relation between the chemical shifts and the proton position

As a first step, we compute the proton position and chemical shift of each solute-solvent configuration to evaluate $\delta_H(\nu)$ in Eq. 2. As shown in Fig. 5, when the proton moves from ν of $\pm$1.1 Å to the center of the hydrogen bond (ν=0), its chemical shift changes from a regular value of 6 ppm to the downfield 23 ppm, demonstrating the sensitivity of δ_H to the fluctuations of the proton positions. Furthermore, while the model molecules have distinct donor and acceptor groups and are in different solvents, their chemical shifts follow the same relation with ν in their SHBs. From a least squares fitting to the data, we obtain a quadratic

Table 1 v_0 and $\langle\delta_H\rangle$ from the AIMD and AI-PIMD simulations of the model molecules. The experimental ^{1}H NMR chemical shifts are included for comparison.

Model molecule	DMANH		HM		DHND	CUA
Solvent	Acetonitrile	Water	Acetone	Water	Water	DMSO
$v_{0,AIMD}$ (Å)	0.42	0.42	0.27	0.34	0.51	-0.54
$v_{0,AI-PIMD}$ (Å)	0.32	0.32	0.23	0.28	0.42	-0.34
$\langle\delta_H\rangle_{AIMD}$ (ppm)	18.9	19.0	20.2	18.9	16.4	17.5
$\langle\delta_H\rangle_{AI-PIMD}$ (ppm)	20.1	20.2	20.3	19.6	17.5	19.6
$\delta_{H,exp}$ (ppm)	18.7[55]	18.5[54]	20.7[44]	20.2[57]	17.7[45]	17.4[56]

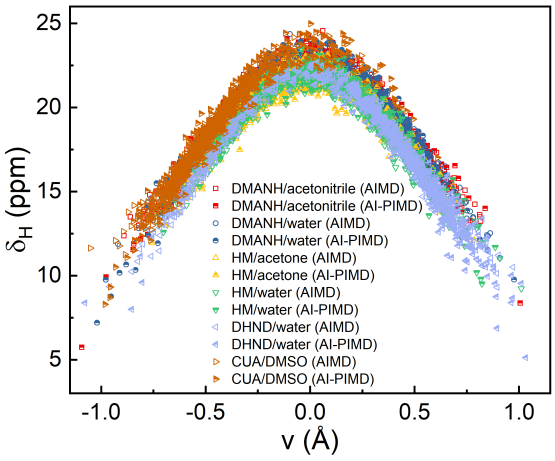

Fig. 5 Correlation plot for δ_H and v. Each data point is calculated from a solute-solvent cluster as sampled from the AIMD and AI-PIMD simulations of the model molecules in different solvents.

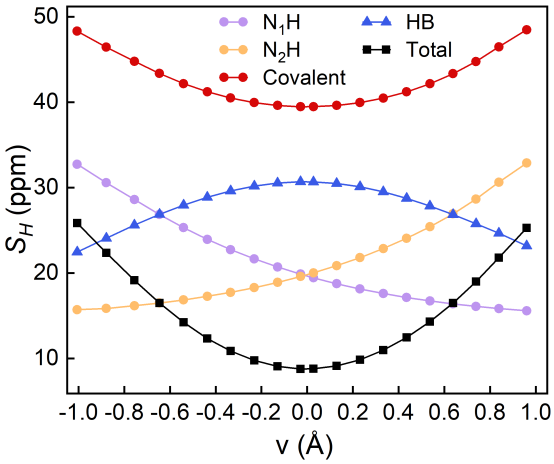

Fig. 6 Decomposition of the total shielding constants into the contributions from covalent bonding (Covalent) and hydrogen bonding (HB) for DMANH.

function for $\delta_H(v)$:

$$\delta_H(v) = 21.9 - 16.1v^2. \quad (3)$$

This observation of a universal trend is consistent with previous experimental and computational studies.[52,53,95–97] In particular, Ceriotti and coworkers have used AI-PIMD simulations to show that the ^{1}H NMR chemical shifts of water in 3 distinct thermodynamic state points fall on the same curve when v is used to represent the proton position in the hydrogen bonds.[96] Compared to their findings that δ_H follows an almost linear relation with the proton position when v is between -1 and 0 Å, here we identify a strong non-linearity for systems containing SHBs.

The ^{1}H NMR chemical shift describes the electronic shielding effect on a proton by the surrounding atoms, which arises from a competition between the covalent bonding and hydrogen bonding interactions in a SHB. We will take the N_1–H$\cdots N_2$ hydrogen bond in DMANH as an example to elucidate how this competition leads to the trend in Fig. 5. For this purpose, we rewrite the chemical shift as $\delta_H = S_{TMS} - S_H$, where S_H is the isotropic magnetic shielding constant for the H atom and S_{TMS} is the shielding constant in the reference compound TMS ($S_{TMS} = 31.6$ ppm from our DFT calculations). Therefore, a downfield chemical shift corresponds to a small shielding constant and vice versa. We then decompose S_H as

$$S_H = S_{N_1H} + S_{N_2H} - S_{HB} = S_{Covalent} - S_{HB}.$$

In the SHB of DMANH, S_{N_1H} and S_{N_2H} are the chemical shielding from the molecular bond between the proton and the N_1 and N_2 atoms, respectively. Their sum gives the overall impact from the covalent bonds, $S_{Covalent}$, which is counteracted by the influence of hydrogen bonding, S_{HB}. To obtain S_{N_1H} and S_{N_2H}, we use N,N-dimethylaniline to mimic the donor and acceptor groups in DMANH and scan the N–H bond length in its protonated form. The value of S_{HB} is then computed by taking the difference between the total shielding constant and $S_{Covalent}$. All of the shielding constants vary with the proton position, and their relations with v are shown in Fig. 6.

When $v < -0.8$ Å, the proton is covalently attached to the N_1 atom in the SHB of DMANH. For example, at v = -1.0 Å, the N_1–H bond length is 0.9 Å and S_{N_1H} has a large value of 32.7 ppm (Fig. 6). To characterize this σ_{NH} bond, we further carry out the NBO analysis[98] to obtain its molecular orbital. As Fig. 7a demonstrates, there is significant amount of electron density between the N_1 and H atoms, which shields the proton from the external magnetic field. Due to the compact structure of this SHB (R = 2.6 Å), the electron density around the N_2 atom also leads to a

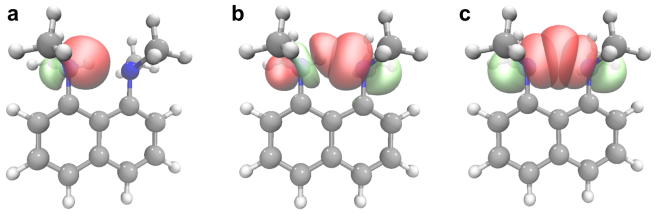

Fig. 7 The natural bond orbitals of DMANH. (a) The σ_{NH} orbital and (b) the overlap of the n_p and σ^*_{NH} orbitals at $\nu = -1.0$ Å. (c) The n_p-s^*_H orbital overlap diagram at $\nu = 0$. Silver, blue and white represent C, N and H atoms, respectively. The red and green spheres are the positive and negative molecular orbitals calculated from the NBO analysis.

σ_{N_2H} of 15.7 ppm, giving an overall $S_{Covalent}$ of 48.4 ppm. In the mean time, the presence of the hydrogen bond induces an opposite effect. As shown in Fig. 7b, while the antibonding σ^*_{NH} orbital contains a nodal plane between the N_1 and H atoms, it has a lobe that points towards the N_2 atom and overlaps with its p-type lone pair orbital, n_p. This leads to a $n_p \rightarrow \sigma^*_{NH}$ charge transfer in the hydrogen bonding interaction and weakens the covalent N_1–H bond. From Fig. 6, The hydrogen bonding interaction deshields the proton by 22.5 ppm and renders a 46% cancellation to the impact of the covalent bonds, giving an overall δ_H of 5.7 ppm. We observe similar competition of these electronic quantum effects in all model molecules, and as a result, their δ_H are in the regular range of 5–10 ppm when $\nu < -0.8$ Å in the SHBs (Fig. 5).

As the proton migrates towards the center of the SHB in DMANH, the covalent bond to the N_1 atom weakens while its new bond with N_2 begins to form. As Fig. 6 shows, this results in a decrease in S_{N_1H} and an increase in S_{N_2H}, with the overall $S_{Covalent}$ reaching a minimum of 39.5 ppm at $\nu = 0$. In this symmetric position, the charge transfer in the hydrogen bonding interaction occurs from the lone pairs of the N_1 and N_2 atoms to the valence s^*_H orbital of the proton, as represented in Fig. 7c. Accordingly, S_{HB} reaches a maximal deshielding of 30.7 ppm (Fig. 6) and the amount of cancellation between the two electronic quantum effects increases to 78%. As shown in Fig. 5, the chemical shift reaches it maximal value of 22.8 ppm. As the chemical structure of DMANH is symmetric, we expect to observe a similar $n_p \rightarrow \sigma^*_{NH}$ charge transfer whenthe proton moves closer to the N_2 atom in the SHB ($\nu > 0$). Therefore, the changes of δ_H and S_H with the proton position in Figs. 5 and 6 exhibit symmetric features with respect to ν =0.

Due to the competition of the covalent and hydrogen bonding interactions, ν makes a good coordinate to characterize δ_H of a SHB. To further examine this observation, we compute the ^{1}H chemical shifts of a network of SHBs in the active site of an enzyme ketosteroid isomerase [19] and compare the results with those from the model small molecules in Fig. S1. In addition, we include the data from previous computational studies that implement DFT methods to calculate the chemical shifts of a variety of organic compounds with intra and intermolecular hydrogen bonds.[99–102] As shown in Fig. S1, the δ_H values follow the same quadratic relation with ν for all systems. While it has been shown that δ_H is strongly correlated with the elongation of the Donor–H covalent bond,[101,103] we find that the universal trend in Figs. 5 and S1 does not hold if we invoke the O–H or N–H bond length, rather than ν, as a coordinate.

3.2.2 Symmetry of the SHBs determines the average chemical shift

From Eq. 2, the average ^{1}H chemical shift of a SHB depends on $\delta_H(\nu)$ and $P(\nu)$. Fig. 5 demonstrates that $\delta_H(\nu)$ of the model molecules follow a universal trend, which can be well described using Eq. 3, despite the differences in their chemical compositions and solvation conditions. Therefore, the variations in $\langle\delta_H\rangle$ observed in Table 1 arise from the probability distribution of ν in the molecules.

From the free energy surfaces in Figs. 2 and 4, we assume that $P(\nu)$ can be written as a linear combination of two Gaussian functions. As detailed in the Supplementary Information, we then insert Eq. 3 in Eq. 2 and obtain the average chemical shift

$$\langle\delta_H\rangle = 20.5 - 16.1\nu_0^2. \quad (4)$$

Here ν_0 is the average proton position in a SHB, which can be calculated from the AIMD and AI-PIMD simulations. Note that the chemical structures of DMANH, HM and DHND are symmetric, and hence one cannot distinguish between the donor and acceptor atoms in their SHBs. In these cases, ν_0 should be taken as the average of the absolute values of ν from the simulations. ν_0 from the AIMD and AI-PIMD simulations of the model molecules are listed in Table 1, and we will use them to assess how the ^{1}H NMR chemical shifts are influenced by the symmetry and quantum nature of the SHBs.

In the model molecules, R of the SHBs are all below 2.7 Å. As shown in Table 1, ν_0 of these systems are mostly below 0.5 Å from the AIMD simulations. Explicit inclusion of nuclear quantum effects allows the proton to move further towards the center of the SHBs and reduces the value of ν_0 by 15-37%. As a result, $\langle\delta_H\rangle$ from the first principles simulations are all above 16 ppm, and the chemical shifts from AI-PIMD simulations are larger by 4–12% than those from AIMD simulations. Therefore, the interplay of electronic and nuclear quantum effects gives rise to the highly downfield ^{1}H NMR chemical shift, a spectral signature of SHBs. Note that in Table 1, in a few cases the $\langle\delta_H\rangle$ values predicted from AIMD and AI-PIMD simulations are larger than those from experimental measurements, as it is well-known that GGA functionals tend to overstructure the hydrogen bonds and overestimate the amount of proton delocalization.[90,104,105] To alleviate the problem, one can use hybrid functionals such as B3LYP[81] in the first principles simulations to better estimate ν_0 and $\langle\delta_H\rangle$.

In the SHBs of DMANH, HM and DHND, the intrinsic ΔpK_a is 0. As Table 1 shows, when DMANH and HM are placed in organic solvents, AI-PIMD simulations predict that $\nu_0 \leq 0.32$ Å and $\langle\delta_H\rangle > 20$ ppm. In contrast, $\langle\delta_H\rangle$ of HM and DHND decrease in aqueous solutions because the heterogeneous solvation environment perturbs their pK_a matched condition and induces asymmetry in their SHBs. Compared to the other 3 model molecules, CUA lacks the reflection symmetry in its chemical structure (Fig. 1) and possesses a ΔpK_a of 3.7 in the SHB. Its ν_0 = -0.34 Å and $\langle\delta_H\rangle$ = 19.6 ppm from the AI-PIMD simulations. To elucidate how

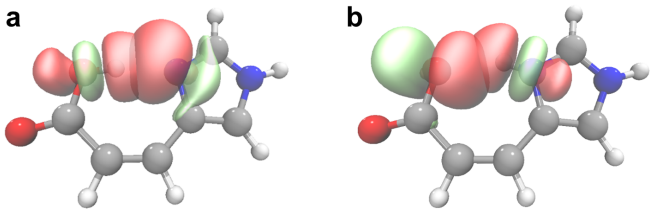

Fig. 8 The n-σ^* orbital overlap diagrams for CUA at (a) v=-0.9 Å and (b) v=1.0 Å. Silver, red and white represent C, O and H atoms, respectively. The red and green spheres are the positive and negative molecular orbitals.

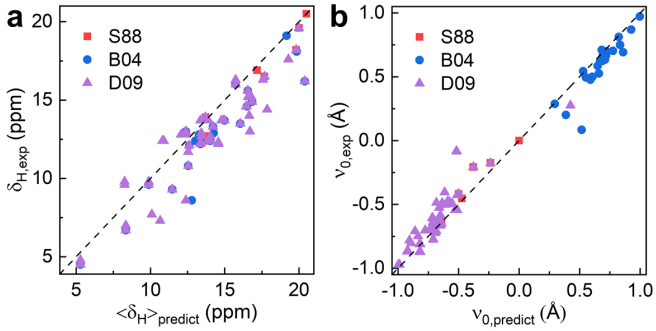

Fig. 9 Comparison between the predicted and experimental[48,52,97] (a) chemical shifts and (b) proton positions of a series of inorganic and organic molecules with SHBs. The dashed diagonal lines represent perfect correlation between the variables.

a non-zero ΔpK_a leads to the asymmetry of a SHB, we carry out the NBO analysis of CUA and evaluate the charge transfer characters when the proton moves between the donor O atom and the acceptor N atom. As shown in Fig. 8a, when v is -0.9 Å, the charge transfer goes from the n_p orbital of the N atom to σ^*_{OH} with substantial orbital overlap. From second-order perturbation theory calculations,[98] this charge delocalization stabilizes the SHB by 24.5 kcal/mol. When the proton is transferred to the N atom, the charge transfer becomes $n_p \rightarrow \sigma^*_{NH}$, as demonstrated in Fig. 8b. However, due to the geometry constraint of the imidazole ring, the σ^*_{NH} orbital points towards the n_p orbital of the O atom with an angle, resulting in a smaller amount of overlap and a reduced stabilization energy of 12.9 kcal/mol. Therefore, ΔpK_a impacts how the electrons are quantum mechanically distributed between the donor and acceptor atoms, which in turn determines the symmetry of the SHB and its ^{1}H NMR chemical shift.

In Eq. 4, one can take ν_0 as the experimentally measured proton position in a SHB. To evaluate its validity, we use the experimental data on a series of inorganic and organic compounds with intra or intermolecular O–H$\cdots$O SHBs, and we refer to the data sets as S88,[48] B04[97] and D09.[52] For these small molecule crystals, the proton positions, $\nu_{0,exp}$, are determined from neutron diffraction and the ^{1}H chemical shifts, $\delta_{H,exp}$, are measured from solid-state NMR spectroscopy. As shown in Fig. 9a, we combine $\nu_{0,exp}$ and Eq. 4 to predict the chemical shifts and find them to be in good agreement with the experimental measurements. As Eq. 4 is developed from the AI-PIMD simulations with the electronic surface described by the BLYP functional, which tends to overly delocalize the protons in the SHBs, it slightly overestimates $\langle\delta_H\rangle$ for a few cases. However, this equation is capable of quantitatively predict the chemical shifts with a root-mean-square deviation of 1.7 ppm as compared to the experimental values. In turn, one can invoke Eq. 4 to derive the proton position in a SHB from the experimental NMR chemical shift. From the 3 data sets, we calculate the ν_0 values and compare them with $\nu_{0,exp}$ in Fig. 9b. The predicted values follow a strong positive correlation with $\nu_{0,exp}$, giving a root-mean-square deviation of 0.1 Å. Therefore, Eq. 4 provides an efficient and accurate way to obtain the location of a proton based on its downfield chemical shift.

4 Conclusions

In this work, we exploit first principles simulations to examine the symmetry and ^{1}H NMR chemical shifts of SHBs, which incorporate the impact of quantum effects and structural and environmental fluctuations on the proton behavior in these compact structures. By performing AIMD and AI-PIMD simulations on a set of model molecules in organic solvents and aqueous solutions, we reveal how the geometrical and chemical criteria required for the formation of symmetric hydrogen bonds reflect the quantum nature of the SHBs. First, the interplay of short R and electronic quantum effects promotes the lengthening of the Donor–H bond and the sharing of the proton in a hydrogen bond. Second, a matched pK_a in a SHB ensures a substantial overlap of the molecular orbitals whether the proton is closer to the donor group or transferred to the acceptor atom, leading to a charge delocalization and stabilization of the hydrogen bonding interaction. Compared to the less polar organic solvents, water molecules have non-uniform interactions with the donor and acceptor atoms in the SHB, which modulates the ΔpK_a value in the hydrogen bond and results in an instantaneous asymmetric distribution of the proton positions. Finally, nuclear quantum effects can qualitatively and quantitatively change the properties of a SHB and hence must be included when considering its symmetry. In particular, the zero-point energy associated with a typical O–H or N–H stretch, which is ~5 kcal/mol at room temperature, allows the proton to be quantum mechanically delocalized and more likely to reside near the center of a hydrogen bond.

While the model molecules have different chemical compositions and solvation environment, Fig. 5 shows that their ^{1}H NMR chemical shifts follow a universal trend with the proton position, which arises from a competition between the covalent bonding and hydrogen bonding interactions. We expect the universal relation in Eq. 3 to hold in SHBs not only in small molecules, but also in biological macromolecules. From the first principles simulations, the proton frequently hops between the donor and acceptor groups with an average residence time less than 1 ps. As such, the ^{1}H chemical shift measured from NMR experiments reflects an ensemble average from a probability distribution of the proton positions, and hence it provides a highly sensitive probe to the symmetry of a SHB. Based on the AI-PIMD simulations and the experimental δ_H of the model molecules, we develop Eq. 4 and uncover why the highly downfield ^{1}H chemical shift is a spectral signature of SHBs.

SHBs occur extensively in proteins and have been proposed

to play essential roles in biological functions.[7–10] However, the geometric features and energetics of these compact structures are still not well understood mainly because of the experimental challenge to determine the proton positions in a large protein.[84,106–108] While neutron diffraction has enabled unambiguous assignment of the proton positions,[9,12,109] its application to macromolecules is limited by the small number of high-flux neutron sources globally.[110] As a result, NMR spectroscopy becomes one of the most commonly used technique in detecting biological SHBs, and the relation between the ^{1}H chemical shift and the hydrogen bond length has been well established.[31,32,47,101] In this work, we demonstrate in Fig. 9b that Eq. 4 allows one to accurately and efficiently calculate the proton position, ν_0, from the chemical shift. Our metric, combined with the previous developed relations, will allow researchers to determine the length and proton position in a SHB directly from NMR measurements, and hence facilitate the investigation of the physical properties and biological functions of these specialized structural elements with unprecedented detail.

Conflicts of interest

There are no conflicts to declare.

5 Acknowledgements

This work is supported by the National Science Foundation through award CHE-1904800. The authors acknowledge the Office of Advanced Research Computing at Rutgers University for providing access to the Amarel and Caliburn servers.

References

1 M. M. Flocco and S. L. Mowbray, *J. Mol. Biol.*, 1995, **254**, 96 – 105.
2 S. Rajagopal and S. Vishveshwara, *FEBS Journal*, 2005, **272**, 1819–1832.
3 S. K. Panigrahi and G. R. Desiraju, *Proteins: Struct., Funct., Bioinf.*, 2007, **67**, 128–141.
4 J. Lin, E. Pozharski and M. A. Wilson, *Biochemistry*, 2017, **56**, 391–402.
5 H. W. Qi and H. Kulik, *J. Chem. Inf. Model.*, 2019, **59**, 2199 – 2211.
6 S. Zhou and L. Wang, *Chem. Sci.*, 2019, **10**, 7734–7745.
7 P. Frey, S. Whitt and J. Tobin, *Science*, 1994, **264**, 1927–1930.
8 W. W. Cleland, P. A. Frey and J. A. Gerlt, *J. Biol. Chem.*, 1998, **273**, 25529–25532.
9 S. Yamaguchi, H. Kamikubo, K. Kurihara, R. Kuroki, N. Niimura, N. Shimizu, Y. Yamazaki and M. Kataoka, *Proc. Natl. Acad. Sci. U.S.A.*, 2009, **106**, 440–444.
10 D. A. Nichols, J. C. Hargis, R. Sanishvili, P. Jaishankar, K. Defrees, E. W. Smith, K. K. Wang, F. Prati, A. R. Renslo, H. L. Woodcock and Y. Chen, *J. Am. Chem. Soc.*, 2015, **137**, 8086–8095.
11 L. M. Oltrogge and S. G. Boxer, *ACS Cent. Sci.*, 2015, **1**, 148–156.
12 P. Kumar, E. H. Serpersu and M. J. Cuneo, *Sci. Adv.*, 2018, **4**, eaas8667.
13 P. Agback and T. Agback, *Sci. Rep.*, 2018, **8**, 10078.
14 M. Pinney, A. Natarajan, F. Yabukarski, D. M. Sanchez, F. Liu, R. Liang, T. Doukov, J. P. Schwans, T. J. Martinez and D. Herschlag, *J. Am. Chem. Soc.*, 2018, **140**, 9827–9843.
15 H. M. Berman, J. Westbrook, Z. Feng, G. Gilliland, T. N. Bhat, H. Weissig, I. N. Shindyalov and P. E. Bourne, *Nucleic Acids Res.*, 1999, **28**, 235–242.
16 P. W. Rose, A. Prlić, A. Altunkaya, C. Bi, A. R. Bradley, C. H. Christie, L. D. Costanzo, J. M. Duarte, S. Dutta, Z. Feng, R. K. Green, D. S. Goodsell, B. Hudson, T. Kalro, R. Lowe, E. Peisach, C. Randle, A. S. Rose, C. Shao, Y.-P. Tao, Y. Valasatava, M. Voigt, J. D. Westbrook, J. Woo, H. Yang, J. Y. Young, C. Zardecki, H. M. Berman and S. K. Burley, *Nucleic Acids Res.*, 2017, **45**, D271.
17 S. J. Grabowski, *Chem. Rev.*, 2011, **111**, 2597–2625.
18 F. Weinhold and R. A. Klein, *Chem. Educ. Res. Pract.*, 2014, **15**, 276–285.
19 L. Wang, S. D. Fried, S. G. Boxer and T. E. Markland, *Proc. Natl. Acad. Sci. U.S.A.*, 2014, **111**, 18454–18459.
20 F. Hibbert and J. Emsley, *Adv. Phys. Org. Chem.*, 1990, **26**, 255 – 379.
21 T. Steiner and W. Saenger, *Acta Cryst. B*, 1994, **50**, 348–357.
22 M. Ichikawa, *Acta Cryst. B*, 1978, **34**, 2074–2080.
23 P. Gilli, V. Bertolasi, V. Ferretti and G. Gilli, *J. Am. Chem. Soc.*, 1994, **116**, 909–915.
24 T. Steiner, *J. Chem. Soc., Chem. Commun.*, 1995, 1331–1332.
25 T. Steiner, *J. Phys. Chem. A*, 1998, **102**, 7041–7052.
26 A. Novak, Large Molecules, Berlin, Heidelberg, 1974, pp. 177–216.
27 N. D. Sokolov, M. V. Vener and V. A. Savel'ev, *J. Mol. Struct.*, 1990, **222**, 365–386.
28 T. Steiner, *Angew. Chem. Int. Ed.*, 2002, **41**, 48–76.
29 G. Gilli and P. Gilli, *J. Mol. Struct.*, 2000, **552**, 1 – 15.
30 R. H. McKenzie, C. Bekker, B. Athokpam and S. G. Ramesh, *J. Chem. Phys.*, 2014, **140**, 174508.
31 T. K. Harris and A. S. Mildvan, *Proteins*, 1999, **35**, 275–282.
32 A. Mildvan, M. Massiah, T. Harris, G. Marks, D. Harrison, C. Viragh, P. Reddy and I. Kovach, *J. Mol. Struct.*, 2002, **615**, 163 – 175.
33 P. A. Sigala, M. A. Tsuchida and D. Herschlag, *Proc. Natl. Acad. Sci. U.S.A.*, 2009, **106**, 9232–9237.
34 P. A. Sigala, J. M. M. Caaveiro, D. Ringe, G. A. Petsko and D. Herschlag, *Biochemistry*, 2009, **48**, 6932–6939.
35 P. Hanoian, P. A. Sigala, D. Herschlag and S. Hammes-Schiffer, *Biochemistry*, 2010, **49**, 10339–10348.
36 P. A. Sigala, E. A. Ruben, C. W. Liu, P. M. B. Piccoli, E. G. Hohenstein, T. J. Martínez, A. J. Schultz and D. Herschlag, *J. Am. Chem. Soc.*, 2015, **137**, 5730–5740.
37 L. Polgár, *Cell. Mol. Life Sci.*, 2005, **62**, 2161–2172.
38 P. A. Frey, *J. Phys. Org. Chem.*, 2004, **17**, 511–520.
39 D. Bao, W. P. Huskey, C. A. Kettner and F. Jordan, *J. Am.*

Chem. Soc., 1999, **121**, 4684–4689.

40 R. W. Alder, P. S. Bowman, W. R. S. Steele and D. R. Winterman, *Chem. Commun.*, 1968, 723–724.

41 R. W. Alder, *Chem. Rev.*, 1989, **89**, 1215–1223.

42 K. Wozniak, H. He, J. Klinowski, T. L. Barr and P. Milart, *J. Phys. Chem.*, 1996, **100**, 11420–11426.

43 P. B. White and M. Hong, *J. Phys. Chem. B*, 2015, **119**, 11581–11589.

44 B. Brzezinski and M. Szafran, *Org. Magn. Reson.*, 1981, **15**, 78–82.

45 Q. Zhao, C. Abeygunawardana, P. Talalay and A. S. Mildvan, *Proc. Natl. Acad. Sci. U.S.A.*, 1996, **93**, 8220–8224.

46 T. K. Harris, Q. Zhao and A. S. Mildvan, *J. Mol. Struct.*, 2000, **552**, 97–109.

47 B. Berglund and R. W. Vaughan, *J. Chem. Phys.*, 1980, **73**, 2037–2043.

48 R. K. Harris, P. Jackson, L. H. Merwin, B. J. Say and G. Hägele, *J. Chem. Soc., Faraday Trans. 1*, 1988, **84**, 3649–3672.

49 A. McDermott and C. F. Ridenour, *Encyclopedia of NMR*, J. Wiley & Sons, Ltd., Sussex, England, 1996, pp. 3820–3825.

50 Q. Zhao, C. Abeygunawardana, A. G. Gittis and A. S. Mildvan, *Biochemistry*, 1997, **36**, 14616–14626.

51 H. Benedict, I. G. Shenderovich, O. L. Malkina, V. G. Malkin, G. S. Denisov, N. S. Golubev and H.-H. Limbach, *J. Am. Chem. Soc.*, 2000, **122**, 1979–1988.

52 H.-H. Limbach, P. M. Tolstoy, N. Pérez-Hernández, J. Guo, I. G. Shenderovich and G. S. Denisov, *Isr. J. Chem.*, 2009, **49**, 199–216.

53 K. Saito and H. Ishikita, *Biochemistry*, 2012, **51**, 1171–1177.

54 L. J. Altman, P. Laungani, G. Gunnarsson, H. Wennerstrom and S. Forsén, *J. Am. Chem. Soc.*, 1978, **100**, 8264–8266.

55 B. Brycki, B. Brzeziński, E. Grech, Z. Malarski and L. Sobczyk, *Magn. Reson. Chem.*, 1991, **29**, 558–560.

56 H. Neuvonen and K. Neuvonen, *J. Chem. Soc., Perkin Trans. 2*, 1998, 1665–1670.

57 J. Lin and P. A. Frey, *J. Am. Chem. Soc.*, 2000, **122**, 11258–11259.

58 R. P. Feynman and A. R. Hibbs, *Quantum Mechanics and Path Integrals*, McGraw-Hill, New York, 1964.

59 D. Chandler and P. G. Wolynes, *J. Chem. Phys.*, 1981, **74**, 4078–4095.

60 B. J. Berne and D. Thirumalai, *Ann. Rev. Phys. Chem.*, 1986, **37**, 401–424.

61 C. R. Groom, I. J. Bruno, M. P. Lightfoot and S. C. Ward, *Acta Cryst. B*, 2016, **72**, 171–179.

62 D. Case, R. Betz, D. Cerutti, T. Cheatham, T. Darden, R. Duke, T. Giese, H. Gohlke, A. Goetz, N. Homeyer, S. Izadi, P. Janowski, J. Kaus, A. Kovalenko, T. Lee, S. LeGrand, P. Li, C. Lin, T. Luchko, R. Luo, B. Madej, D. Mermelstein, K. Merz, G. Monard, H. Nguyen, H. Nguyen, I. Omelyan, A. Onufriev, D. Roe, A. Roitberg, C. Sagui, C. Simmerling, W. Botello-Smith, J. Swails, R. Walker, J. Wang, R. Wolf, X. Wu, L. Xiao and P. Kollman, *AMBER 2016*, University of California, San Francisco, 2016.

63 J. Wang, R. M. Wolf, J. W. Caldwell, P. A. Kollman and D. A. Case, *J. Comput. Chem.*, 2004, **25**, 1157–1174.

64 W. W. L. Jorgensen, J. Chandrasekhar, J. D. Madura, R. W. Impey and M. L. Klein, *J. Chem. Phys.*, 1983, **79**, 926.

65 J.-P. Ryckaert, G. Ciccotti and H. J. Berendsen, *J. Comput. Phys.*, 1977, **23**, 327 – 341.

66 T. Darden, D. York and L. Pedersen, *J. Chem. Phys.*, 1993, **98**, 10089–10092.

67 R. J. Loncharich, B. R. Brooks and R. W. Pastor, *Biopolymers*, 1992, **32**, 523–535.

68 H. J. C. Berendsen, J. P. M. Postma, W. F. Van Gunsteren, A. DiNola and J. R. Haak, *J. Chem. Phys.*, 1984, **81**, 3684.

69 J. VandeVondele, M. Krack, F. Mohamed, M. Parrinello, T. Chassaing and J. Hutter, *Comp. Phys. Comm.*, 2005, **167**, 103–128.

70 V. Kapil, M. Rossi, O. Marsalek, R. Petraglia, Y. Litman, T. Spura, B. Cheng, A. Cuzzocrea, R. H. Meißner, D. M. Wilkins, B. A. Helfrecht, P. Juda, S. P. Bienvenue, W. Fang, J. Kessler, I. Poltavsky, S. Vandenbrande, J. Wieme, C. Corminboeuf, T. D. Kühne, D. E. Manolopoulos, T. E. Markland, J. O. Richardson, A. Tkatchenko, G. A. Tribello, V. Van Speybroeck and M. Ceriotti, *Comput. Phys. Commun.*, 2019, **236**, 214–223.

71 A. D. Becke, *Phys. Rev. A*, 1988, **38**, 3098.

72 C. Lee, W. Yang and R. G. Parr, *Phys. Rev. B*, 1988, **37**, 785.

73 S. Grimme, J. Antony, S. Ehrlich and H. Krieg, *J. Chem. Phys.*, 2010, **132**, 154104.

74 S. Goedecker, M. Teter and J. Hutter, *Phys. Rev. B*, 1996, **54**, 1703–1710.

75 G. Bussi, D. Donadio and M. Parrinello, *J. Chem. Phys.*, 2007, **126**, 14101.

76 M. Ceriotti and D. E. Manolopoulos, *Phys. Rev. Lett.*, 2012, **109**, 100604.

77 London, F., *J. Phys. Radium*, 1937, **8**, 397–409.

78 R. Ditchfield, *Mol. Phys.*, 1974, **27**, 789–807.

79 K. Wolinski, J. F. Hinton and P. Pulay, *J. Am. Chem. Soc.*, 1990, **112**, 8251–8260.

80 M. J. Frisch, G. W. Trucks, H. B. Schlegel, G. E. Scuseria, M. A. Robb, J. R. Cheeseman, G. Scalmani, V. Barone, G. A. Petersson, H. Nakatsuji, X. Li, M. Caricato, A. V. Marenich, J. Bloino, B. G. Janesko, R. Gomperts, B. Mennucci, H. P. Hratchian, J. V. Ortiz, A. F. Izmaylov, J. L. Sonnenberg, D. Williams-Young, F. Ding, F. Lipparini, F. Egidi, J. Goings, B. Peng, A. Petrone, T. Henderson, D. Ranasinghe, V. G. Zakrzewski, J. Gao, N. Rega, G. Zheng, W. Liang, M. Hada, M. Ehara, K. Toyota, R. Fukuda, J. Hasegawa, M. Ishida, T. Nakajima, Y. Honda, O. Kitao, H. Nakai, T. Vreven, K. Throssell, J. A. Montgomery, Jr., J. E. Peralta, F. Ogliaro, M. J. Bearpark, J. J. Heyd, E. N. Brothers, K. N. Kudin, V. N. Staroverov, T. A. Keith, R. Kobayashi, J. Normand, K. Raghavachari, A. P. Rendell, J. C. Burant, S. S. Iyengar, J. Tomasi, M. Cossi, J. M. Millam, M. Klene, C. Adamo, R. Cammi, J. W. Ochterski, R. L. Martin, K. Morokuma,

O. Farkas, J. B. Foresman and D. J. Fox, *Gaussian 16 Revision A.03*, 2016, Gaussian Inc. Wallingford CT.
81 A. D. Becke, *J. Chem. Phys.*, 1993, **98**, 5648.
82 E. D. Glendening, C. R. Landis and F. Weinhold, *J. Comput. Chem.*, 2013, **34**, 1429–1437.
83 C. L. Perrin, *Science*, 1994, **266**, 1665.
84 C. L. Perrin, *Acc. Chem. Res.*, 2010, **43**, 1550–1557.
85 Y. Masuda, Y. Mori and K. Sakurai, *J. Phys. Chem. A*, 2013, **117**, 10576–10587.
86 A. Jezierska and J. J. Panek, *J. Chem. Inf. Model.*, 2015, **55**, 1148–1157.
87 S. Habershon, T. E. Markland and D. E. Manolopoulos, *J. Chem. Phys.*, 2009, **131**, 24501.
88 X.-Z. Li, B. Walker and A. Michaelides, *Proc. Natl. Acad. Sci. USA*, 2011, **108**, 6369–6373.
89 T. E. Markland and B. J. Berne, *Proc. Natl. Acad. Sci. U.S.A.*, 2012, **109**, 7988–7991.
90 M. Ceriotti, W. Fang, P. G. Kusalik, R. H. McKenzie, A. Michaelides, M. A. Morales and T. E. Markland, *Chem. Rev.*, 2016, **116**, 7529–7550.
91 W. Fang, J. Chen, M. Rossi, Y. Feng, X.-Z. Li and A. Michaelides, *J. Phys. Chem. Lett.*, 2016, **7**, 2125–2131.
92 P. Dopieralski, C. L. Perrin and Z. Latajka, *J. Chem. Theory Comput.*, 2011, **7**, 3505–3513.
93 J. D. Roberts, C. Yu, C. Flanagan and T. R. Birdseye, *J. Am. Chem. Soc.*, 1982, **104**, 3945–3949.
94 M. Garcia-Viloca, A. González-Lafont and J. Lluch, *J. Am. Chem. Soc.*, 1999, **121**, 9198–9207.
95 A. A. Hassanali, J. Cuny, M. Ceriotti, C. J. Pickard and M. Parrinello, *J. Am. Chem. Soc.*, 2012, **134**, 8557–8569.
96 M. Ceriotti, J. Cuny, M. Parrinello and D. E. Manolopoulos, *Proc. Natl. Acad. Sci. USA*, 2013, **110**, 15591–6.
97 T. Emmler, S. Gieschler, H. H. Limbach and G. Buntkowsky, *J. Mol. Struct.*, 2004, **700**, 29–38.
98 A. E. Reed, L. A. Curtiss and F. Weinhold, *Chem. Rev.*, 1988, **88**, 899–926.
99 A. V. Afonin, I. A. Ushakov, L. N. Sobenina, Z. V. Stepanova, O. V. Petrova and B. A. Trofimov, *Magn. Reson. Chem.*, 2006, **44**, 59–65.
100 M. G. Siskos, V. G. Kontogianni, C. G. Tsiafoulis, A. G. Tzakos and I. P. Gerothanassis, *Org. Biomol. Chem.*, 2013, **11**, 7400–7411.
101 M. G. Siskos, A. G. Tzakos and I. P. Gerothanassis, *Org. Biomol. Chem.*, 2015, **13**, 8852–8868.
102 M. G. Siskos, M. I. Choudhary and I. P. Gerothanassis, *Org. Biomol. Chem.*, 2017, **15**, 4655–4666.
103 B. G. Pfrommer, F. Mauri and S. G. Louie, *J. Chem. Am. Soc.*, 2000, **122**, 123–129.
104 J. A. Morrone and R. Car, *Phys. Rev. Lett.*, 2008, **101**, 17801.
105 L. Wang, M. Ceriotti and T. E. Markland, *J. Chem. Phys.*, 2014, **141**, 104502.
106 A. Warshel, A. Papazyan and P. Kollman, *Science*, 1995, **269**, 102–106.
107 A. Warshel and A. Papazyan, *Proc. Natl. Acad. Sci. U.S.A.*, 1996, **93**, 13665–13670.
108 E. L. Ash, J. L. Sudmeier, E. C. De Fabo and W. W. Bachovchin, *Science*, 1997, **278**, 1128.
109 K. Yonezawa, N. Shimizu, K. Kurihara, Y. Yamazaki, H. Kamikubo and M. Kataoka, *Scientific Reports*, 2017, **7**, 9361.
110 E. Oksanen, J. C.-H. Chen and S. Z. Fisher, *Molecules*, 2017, **22**, 596.

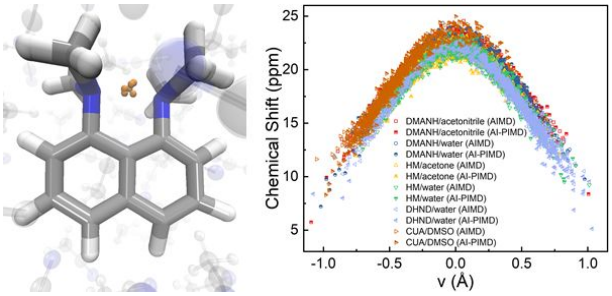

Electronic and nuclear quantum effects determine the symmetry and highly downfield ^{1}H NMR chemical shifts of short hydrogen bonds.